Wicking Properties of Various Polyamide Nanofibrous Structures with an Optimized Method

Bert De Schoenmaker, Lien Van der Schueren, Sander De Vrieze, Philippe Westbroek, Karen De Clerck

Department of Textiles, Ghent University, Technologiepark 907, B-9052 Ghent, Belgium

Received 3 June 2010; accepted 1 August 2010
DOI 10.1002/app.33117
Published online 13 October 2010 in Wiley Online Library (wileyonlinelibrary.com).

ABSTRACT: In comparison with conventional structures, nanofibrous structures have unique characteristics, such as higher surface-to-volume ratios, smaller pores, and higher porosity. Their hydrophilic nature is a key characteristic for many applications. However, because of their high porosity, it is difficult to measure the hydrophilicity of nanofibrous structures with contact-angle measurements. Therefore, characterization through wicking behavior is more appropriate. The International Organization for Standardization norm on wicking needs some refining to account for the specific nature of highly porous nanofibrous structures. A refined method was used on several structures that differed in the fiber diameter and the polyamide type. The structures with the thickest nanofibers had the highest wicking rates. At equilibrium, the wicking heights of structures of different polyamide types with the same average fiber diameter followed the trend expected from their intrinsic hydrophilicity. In the initial phase, the capillary forces established the wicking behavior. Later in the process, the wicking behavior was determined by the capillary forces and the hydrophilicity. In conclusion, the hydrophilicity of nanofibrous structures can be successfully determined by an optimized wicking procedure, and the fiber diameter is the dominant parameter for the resulting wicking height at equilibrium. © 2010 Wiley Periodicals, Inc. J Appl Polym Sci 120: 305–310, 2011

Key words: membranes; nanofiber; polyamides; wicking behavior

INTRODUCTION

Recently, nanotechnology has become an interesting field in all scientific domains. Within the domain of textiles, the development of nanofibers through electrospinning is an important breakthrough with many possible applications. By definition, nanofibers have a diameter that is less than 500 nm; even fibers with diameters of a few nanometers have been reported.[1] Because their length can reach several kilometers, these fibers provide a connection between the nanoscale world and the macroscale world.

Nanofibers are commonly obtained by solvent electrospinning. A polymer solution is pumped at a constant flow rate through a nozzle in an electric field, which is applied between the nozzle tip of the polymer reservoir and the collector plate. When the electrostatic forces overcome the surface tension of the solution, the droplet at the outlet of the needle deforms into a Taylor cone. From this moment, a jet stream is drawn out of the Taylor cone. Because of the interaction of the charges inherent to the solution and the external electric field, this jet is subjected to bending and splaying. As a result, fine fibers are randomly deposited onto the collector plate, and a nonwoven structure is formed.

When the diameter is reduced to less than 500 nm, several specific and unique characteristics appear. In contrast to macroscale nonwovens, these nanoscale structures have larger specific surface-to-volume ratios (up to 100 m^2/g), higher porosity (up to 90%), and smaller pore sizes (50–200 nm). Because the roughness of nanofiber mats is determined on the nanolevel, they have a very flat surface.[2] Also, the mechanical performance is superior to that of other forms of the same material.[3] Because of the large specific surface area, these structures absorb fluids very efficiently.[4] Other important properties are malleability[5] and ease of fiber modification.[6]

Because of this variety of properties, many applications have been suggested. Nanofibrous mats are used in biomedical applications[7] such as prostheses, tissue templates, wound dressings, and drug-release systems. Electrospun nanofibers can also be applied in protective clothing,[8] composites,[1] and electrical and optical applications.[9] Because the filter efficiency is directly related to the fiber fineness, filtration is another promising application.[10]

For many of the aforementioned applications, a good understanding of the liquid absorption and

Correspondence to: K. De Clerck (karen.declerck@ugent.be).

wettability of nanofibrous mats is crucial. However, only a few studies of this subject have been published. Jabal et al.[11] investigated the hydrophilicity of poly(vinylpyrrolidone)–titania nanofibers with contact-angle measurements.[11] Zhang et al.[12] did the same for cellulose nanofibers, and Chen et al.[13] studied the hydrophilicity of thermoplastic polyurethane/collagen blends. Conclusions on hydrophilicity based on contact-angle measurements are based on adhesion principles, but the water drop uptake behavior of nanofibrous structures is more complex because of the specific characteristics of nanofibers and is determined from the following:

- The properties of adhesion between the polymeric material and water.
- The capillary forces due to the small pore sizes.
- The high porosity of the membranes (which allows the soaking of a large amount of liquid).

As a result, contact-angle measurements alone do not allow for a full understanding of the hydrophilicity of nanofibrous materials. Therefore, the wicking method has been proposed as a complementary method. It is believed that this method offers a solution to some of the shortcomings of contact-angle measurements for nanofibrous structures. In a wicking procedure, the absorption height of the liquid is recorded as a function of time. Wicking is a spontaneous process by which the fiber–air interface is replaced by a fiber–liquid interface, and the height that the liquid reaches is determined by the capillary force, which overcomes gravity forces. Additionally, interfacial forces between the polymer material and the liquid also play a role.

The wicking rate of a liquid in a porous structure is given by Poiseuille's law:[14]

$$\frac{dh}{dt} = \frac{R_D^2}{8\eta h}\left(\frac{2\gamma\cos\theta}{R_S} - \rho g h\right) = \frac{R_D^2}{8\eta h}\Delta P \qquad (1)$$

where h is the height of the liquid at time t; η, ρ, and γ are the viscosity, density, and surface tension of the liquid, respectively; θ is the advancing contact angle of the liquid on the surface; g is the acceleration due to gravity; R_D is the mean hydrodynamic radius of the pores; and R_S is the mean static radius of the pores, which is equal to the geometrical radius of the pores. The hydrodynamic radius also depends on the tortuosity of the pores.[15]

The pressure difference (ΔP) is composed of the capillary pressure and the pressure due to gravity. In the early stages of the wicking phenomenon, the hydrostatic pressure can be neglected, and the Washburn equation can be yielded by the integration of Eq. (1):

$$h^2 = \frac{r\gamma\cos\theta}{2\eta} \qquad (2)$$

where $r = R_D{}^2/R_S$ is an equivalent radius of the capillary porous structure.

Hence, h^2 values must vary linearly with time in the initial phase of the process:

$$h^2 = Dt \qquad (3)$$

where D is a capillary diffusion coefficient related to the pore size and the properties of the liquid.[16]

Hong and Kang[16] already performed wicking experiments on electrospun structures, but they showed diameters in the microscale range. Moreover, their research focused on the differences between conventional nonwovens and electrospun nonwovens. However, for a full understanding of the wicking behavior of nanofibrous structures, it would be interesting to compare nanofibrous structures with different characteristics. In this work, the wicking behavior of polyamide (PA) nanofibrous structures was studied. The influence of the diameter was investigated through the testing of nanofibrous structures with diameters in the range of 140–340 nm. To determine the influence of the intrinsic liquid absorption capacity in the bulk phase on the wicking behavior of the resulting nanofibrous structures, four different PA types were used: PA6, PA6.6, PA6.9, and PA4.6.

EXPERIMENTAL

Materials

As a reference material, a spin-bound nonwoven of PA6.6 (fiber diameter = 17 μm, porosity = 85%; Ensait, Lille, France) was used. PA6, PA4.6, and PA6.6 pellets were obtained from Sigma–Aldrich. PA6.9 pellets were obtained from Scientific Polymer Products, Canada. The electrospinning solvents, 99.8% acetic acid and 98–100% formic acid, were also delivered by Sigma–Aldrich. The dye methylene blue was purchased from Sigma–Aldrich.

Methods

To obtain uniform nanofiber mats, a multinozzle electrospinning setup was used; this is an in-house-developed technology and has been described elsewhere.[17] This multinozzle method diverges from a mononozzle setup only in the number of nozzles; the general methodology itself is the same. Six nozzles, each fed by a syringe, are placed in two alternating rows on a plate that has movement in the width direction. In the meantime, a collector is moving in the production direction. The thickness of the samples can be adapted by the speed of this collector, but it was kept constant during this study. With this multinozzle setup, the nanofibrous structures that were produced were large enough allow for the wicking strips to be cut from one fabric batch.

Table I presents the six structures electrospun for this research. All the nanofiber mats were electrospun

TABLE I
Properties of the electrospun nanofibrous structures analysed in this work

Polyamide type	Molecular weight	Weight percentage [wt%]	Viscosity [cP]	Average fibre diameter [nm]	Web density [g/m^2]
PA 6	50.000	14	293.3	145 ± 16	51,44
PA 6	50.000	16	514.4	160 ± 15	55,36
PA 6	50.000	20	1864	340 ± 28	50,49
PA 6.6	60.000	14	493.4	143 ± 29	60,16
PA 6.9	60.000	14	407.3	170 ± 25	42,43
PA 4.6	80.000	14	746.1	203 ± 18	50.32

from a 1 : 1 formic acid/acetic acid solution. The polymer concentration used to produce each mat is listed in Table I. Through the variation of the polymer concentration, structures with different average fiber diameters were produced. The viscosities were measured with a Brookfield LVDV-II+ Pro (Middleboro, Massachusetts) at a share rate of 5.28; for the 20 wt % PA6, however, a share rate of 1.98 was used.

The tip-to-collector distance was set to 6 cm, and the flow rate was 2 mL/h; however, for 20 wt % PA6, the flow rate was 1.5 mL/h. The voltage was adjusted between 25 and 30 kV to obtain steady-state conditions.[18]

The web density, which is also listed in Table I, was measured with the International Organization for Standardization (ISO) 9864 norm. The measurements were performed in a conditioned room at 296 K with a relative humidity of 50%.

The fiber morphology of the samples was examined by scanning electron microscopy with a Fei Quanta 200F system (Hillsboro, Oregon). Before the scanning electron microscopy measurements, the nanofibrous structures were coated with a gold sputter coater (SCD 030, Balzers Union, Liechtenstein). The fiber diameters were measured with Cell^D software (Olympus, Southend-on-Sea, UK); 60 measurements were used to determine the average fiber diameter of each structure.

A specific norm for the measurement of the wicking phenomenon in nanofibrous structures does not exist, so as a starting point, the norm for textile nonwovens (ISO 9073-6) was applied. All samples were conditioned for 24 h at a temperature of 296 K and a relative humidity of 50%. Nanofibrous strips (15 × 150 mm^2) were clamped vertically onto a horizontal support that was parallel to a vertical millimeter rod, which was placed 15 mm above the lower end of the sample. A water basin was raised with a laboratory jack until the liquid surface touched the millimeter rod. The lower sample end was thus 15 mm below the liquid surface during the experiment. A stopwatch was started as soon as the liquid surface touched the measuring rod. The height of the capillary rise was recorded as a function of time. All wicking experiments were performed at 296 K and 50% relative humidity.

RESULTS AND DISCUSSION

Optimization of the wicking setup

Because preliminary research showed that the nanofibrous membranes had different tensile strengths in the production and cross directions, wicking tests were performed in both directions. Figure 1 clearly shows that there was no significant influence of the direction on the wicking behavior of the nanofibrous structures. Moreover, the porosity and pore size were not dependent on the direction. Further experiments are thus reported only for the cross direction.

Although ISO 9073-6 describes how wicking should be determined for standard nonwoven textile structures, it is not very useful for nanofibrous structures. In this norm, the wicking height is detected through the uptake of a colored liquid with a dye, which was in this case methylene blue. Performing wicking tests with the colored liquid and water on nanofibrous structures revealed that there was a significant difference in the wicking heights of the colored and uncolored liquids. Figure 2 clearly shows that with a colored liquid (as described in the related ISO norm), the wicking height was significantly lower than the real height of the water in the

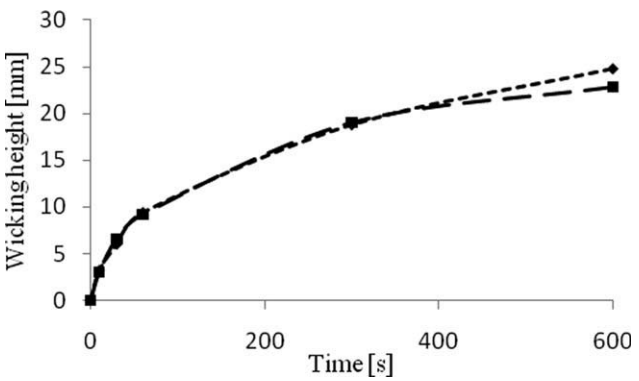

Figure 1 Wicking height of PA6 nanofibrous structures (◆) along the production direction and (■) in the cross direction of the production direction.

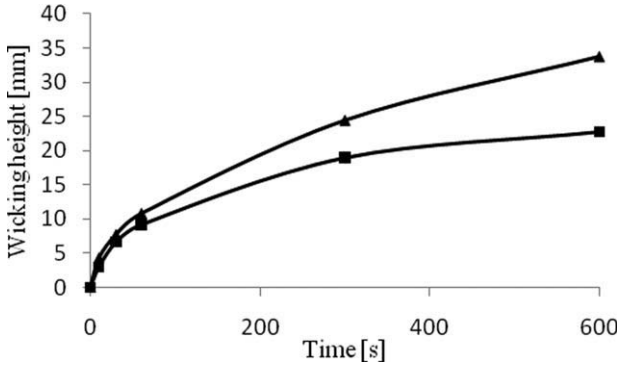

Figure 2 Wicking height of PA6 nanofibrous structures along the cross direction of the production direction (■) with a dye and (▲) without a dye.

nanofibrous structures. The underestimation was almost 30% of the real liquid height. The interaction between the dye molecules (ISO 9073-6) and the fine nanofibers was high and resulted in adsorption of the dye at the nanofiber surface. Because of this dye time lag, the dye front was not a good indicator of the liquid height. Therefore, the method was altered in this research, and pure demineralized water was used. A strong lamp (KL 1500 LCD, Olympus) was applied to follow the actual wicking height.

Difference between the conventional spin-bound nonwovens and the electrospun nanofibrous structures

The difference in wicking behavior between a PA6.6 microfiber nonwoven (with an average fiber diameter of 17 μm) and a nanofibrous structure (with an average fiber diameter of 145 nm) is reported in Figure 3. The wicking height of the nanofibrous structure was 4 times greater than that of the conventional nonwoven structure. This result is in agreement with the literature on PA6 fibrous structures.[18] Because of the smaller pore size of the electrospun nanofibrous structures, ΔP in Eq. (1) was larger; this resulted in a higher capillary force and a higher wicking height and rate.

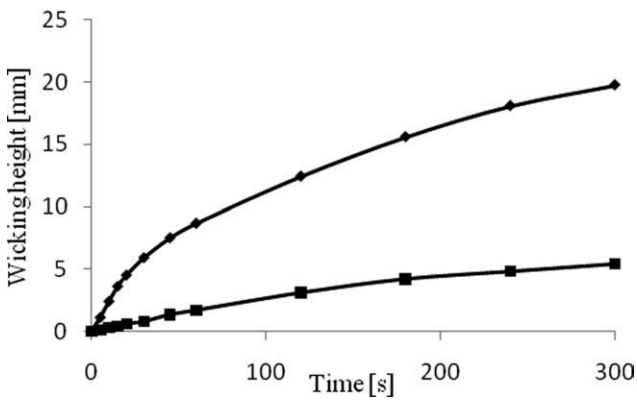

Figure 3 Wicking behavior of (■) a PA6.6 spin-bound nonwoven and (◆) a PA6.6 electrospun nanofibrous structure.

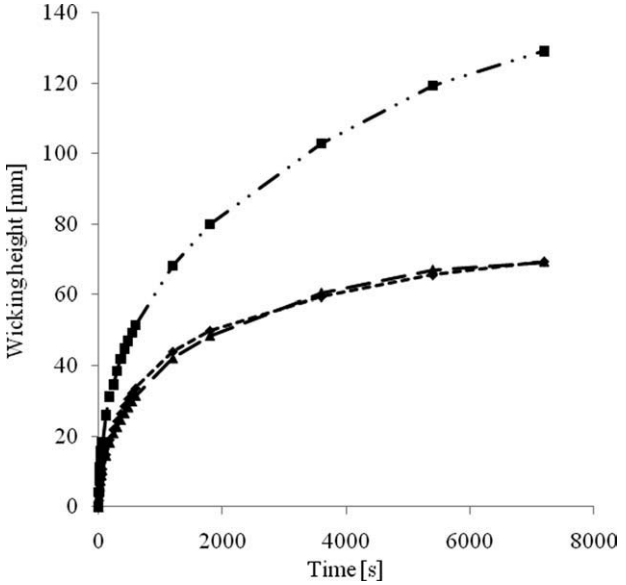

Figure 4 Influence of the fiber diameter on the wicking behavior of PA6 nanofibrous structures with diameters of (▲) 145, (◆) 160, and (■) 340 nm.

Influence of the nanofiber diameter

We produced electrospun PA6 nanofibrous structures with different fiber diameters (see Table I) to investigate the influence of the diameter on the wicking rate and height. All nanofibrous structures consisted of the same material, were produced on the same machine under the same processing conditions, and possessed the same weight. The only difference between the three structures was the fiber diameter. In Figure 4, the wicking heights of the nanofibrous structures with diameters of 145, 160, and 340 nm are shown. The wicking height of the structures with a diameter of 340 nm was significantly higher than the wicking heights of the structures with diameters of 145 of 160 nm. Within the nanofibrous structures, the wicking height thus increased with increasing fiber diameter. Earlier, however, it was shown that a conventional nonwoven has a lower wicking height than a nano-nonwoven of the same material, which has a smaller average fiber diameter. Thus, in the nanorange, an increase in the fiber diameter has a positive influence on the wicking behavior; when this nano-area is left, the capillary forces decrease a lot, and a lower wicking height results.

This behavior occurred not only at equilibrium when the maximum wicking height was obtained but also in the initial stage of the process when Eq.

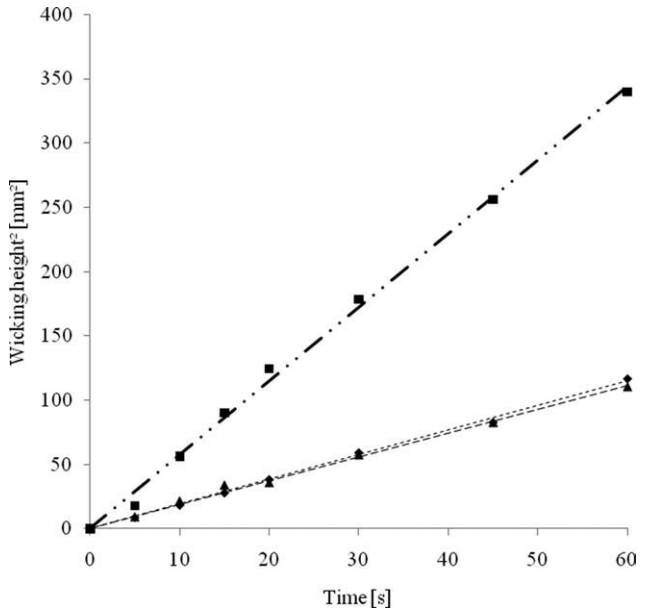

Figure 5 Square height of the capillary rise on PA6 nanofibrous structures with fiber diameters of (▲) 145, (◆) 160, and (■) 340 nm.

(2) was valid. The data are plotted in Figure 5 and show linear behavior between h^2 and time as predicted by eqs. (2) and (3). The measuring points very well follow the straight line, so the Washburn approach is highly satisfactory.

D corresponds to the slope of the Washburn curve. The *D* values for the different PA6 nanofibrous structures are presented in Table II. The *D* values were similar for the nanofibrous structures with average fiber diameters of 145 and 160 nm. This indicated that, when the standard deviation of the diameter was taken into account, there was no statistical difference between the nanofibrous structures. However, the diffusion coefficient of the 340-nm structure was almost 3 times higher, and this indicated that the water level uptake rate in the nanofibrous structure was 3 times higher than the rate in the nanofibrous structures with diameters of 145 and 160 nm.

Influence of the PA type

The influence of the material properties on the wicking behavior was examined through the study of four different types of PA nanofibrous nonwovens with similar fiber diameters (PA6, PA6.6, PA4.6, and PA6.9). Figure 6 shows the wicking data obtained for the PA6 and PA6.6 nanofibrous structures with an average diameter of 145 nm, for PA6.9 with an average diameter of 160 nm, and for PA4.6 with an average fiber diameter of 200 nm. PA4.6 possessed the highest wicking height at equilibrium, whereas the wicking height of PA6.9 was approximately 20 mm less. This was in agreement with the water absorption capacity of the bulk materials of these PAs (2.3% for PA4.6, 1.5% for PA6, 1.2% for PA6.6, and 0.48% for PA6.9). Because the PA4.6 nanofibers were indeed more hydrophilic, the resistance against the rising of the liquid to a higher level into the structure decreased. Moreover, although the PA6.9 structure had the second thickest fibers, it had the lowest wicking height because of its low water absorption capacity in the bulk phase, which resulted in high resistance against the rising of water. Thus, it can be concluded that at equilibrium, the properties of the material overshadow the capillary forces.

TABLE II
***D* Values of the Different PA6 Nanofibrous Structures**

Nonwoven	*D* value
145-nm PA6	1.87
160-nm PA6	1.91
340-nm PA6	5.74

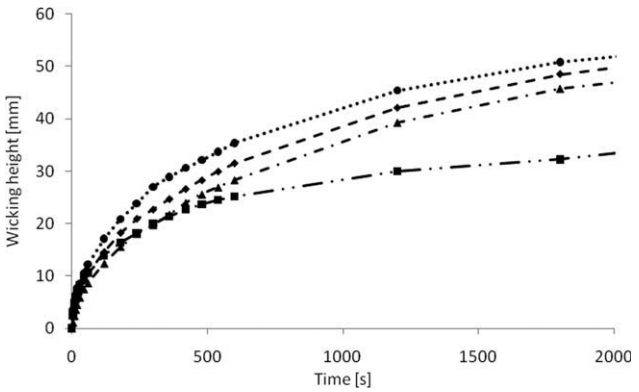

Figure 6 Wicking height of nanofibrous structures of (■) PA6 and (▲) PA6.6 with a fiber diameter of 145 nm, (◆) PA6.9 with a fiber diameter of 165 nm, and (●) PA4.6 with a fiber diameter of 200 nm.

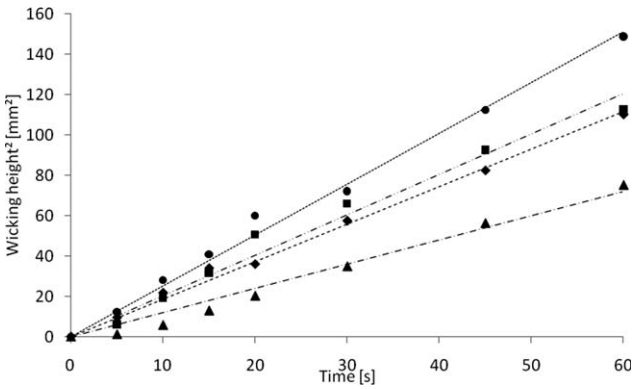

Figure 7 Square height of the capillary rise on nanofibrous structures of (■) PA6 with a fiber diameter of 145 nm, (▲) PA6.6 with a fiber diameter of 145 nm, (◆) PA6.9 with a fiber diameter of 165 nm, and (●) PA4.6 with a fiber diameter of 200 nm.

TABLE III
***D* Values of the Different PA Nanofibrous Structures**

Nonwoven	*D* value
PA6	1.87
PA6.6	1.20
PA6.9	2.01
PA4.6	2.52

The wicking rate in the first minute is shown in Figure 7. The structure with the highest wicking rate remained PA4.6. Although PA6.9 was more hydrophobic in the bulk phase, its wicking rate was higher than the initial rates of PA6 and PA6.6. This could be explained by the thicker fibers of the PA6.9 structure, which caused larger pores. Because of these larger pores, there was less interface between the liquid and fibers, so there was less resistance against the rising of the liquid to a higher level into the structure. This is in agreement with the Washburn equation [Eq. (2)]. Thus, during the first stages, the capillary force is the driving factor, whereas at a later stage in the wicking process, the material properties become the dominant factor.

Table III presents the *D* values of the different PA types. The lower water absorption capacity of PA6.6 accounted for the lower *D* value of the nanofibrous structure versus the PA6 structure. Pursuing this explanation for the PA6.9 structure, we found that the *D* value should be even lower than that for the PA6.6 structure. The higher *D* value of the PA6.9 nanofibrous structure was attributed to the higher fiber diameter of the structure.

CONCLUSIONS

An optimized method for examining the wicking behavior of nanofibrous structures has been developed. To allow the measurement of the real liquid height, a strong lamp is used instead of a dye. The wicking height of nanofibrous structures is significantly higher than the height of spin-bound nonwovens. According to a comparison of different nanofibrous structures, the highest wicking rates are obtained with the nanofibrous structures with the thickest nanofibers and thus with the largest pore sizes. However, above this nanoscale diameter, the fibers become too thick, and the wicking rate will decrease with increasing fiber diameter. During the initial phase of the wicking experiment, the capillary forces, determined mainly by the fiber diameter, establish the wicking rate. Later in the process, the height is determined by the capillary force as well as the hydrophilicity of the PA type.

References

1. Huang, C.; Chen, S.; Lai, C.; Reneker, D. H.; Qiu, H.; Ye, Y.; Hou, H. Nanotechnology 2006, 17, 1558.
2. De Vrieze, S. J Mater Sci 2007, 42, 8029.
3. Huang, Z.-M.; Zhang, Y.-Z.; Kotaki, M.; Ramakrishna, S. Compos Sci Technol 2003, 63, 2223.
4. Fang, J.; Niu, H. T.; Lin, T.; Wang, X. G. Chin Sci Bull 2008, 53, 2265.
5. Liang, D.; Hsiao, B. S.; Chu, B. Adv Drug Delivery Rev 2007, 59, 1392.
6. Yoo, H. S.; Kim, T. G.; Park, T. G. Adv Drug Delivery Rev 2009, 61, 1033.
7. Agarwal, S.; Wendorff, J. H.; Greiner, A. Polymer 2008, 49, 5603.
8. Smidt, D.; Reneker, D. H. PCT/U.S. Pat. 00/27737 (2001).
9. Norris, I. D. Synth Met 2000, 114, 109.
10. Gopal, R.; Kaur, S.; Ma, Z.; Chan, C.; Ramakrishna, S.; Matsuura, T. J Membr Sci 2006, 281, 581.
11. Jabal, J. M. F. et al. Am Chem Soc Appl Mater Interfaces 2009, 1, 2325.
12. Zhang, H. T. Mater Lett 2009, 63, 1199.
13. Chen, R.; Qiu, L.; Ke, Q.; He, C.; Mo, X. J Biomater Sci Polym Ed 2009, 20, 1513.
14. Chen, X. et al. Text Res J 2009, 76, 1364.
15. Ferrero, F. Polym Test 2003, 22, 571.
16. Hong, K. H.; Kang, T. J. J Appl Polym Sci 2006, 100, 167.
17. Westbroek, P.; Van Camp, T.; De Vrieze, S.; De Clerck, K. PCT/Eur. Pat. 2008/056050 (2008).
18. De Vrieze, S. et al. J Appl Polym Sci 2009, 115, 837.